

Review

# Bone mineralization density distribution in health and disease

P. Roschger<sup>a</sup>, E.P. Paschalis<sup>a</sup>, P. Fratzl<sup>b</sup>, K. Klaushofer<sup>a,\*</sup>

<sup>a</sup> Ludwig Boltzmann Institute of Osteology at Hanusch Hospital of WGKK and AUVA Trauma Centre Meidling, 4th Medical Department, Hanusch Hospital, Heinrich Collin Street 30, A-1140, Vienna, Austria

<sup>b</sup> Max Planck Institute of Colloids and Interfaces, Department of Biomaterials, Potsdam, Germany

Received 8 October 2007; accepted 28 October 2007

Available online 12 November 2007

## Abstract

Human cortical and trabecular bones are formed by individual osteons and bone packets, respectively, which are produced at different time points during the (re)modeling cycle by the coupled activity of bone cells. This leads to a heterogeneously mineralized bone material with a characteristic bone mineralization density distribution (BMDD) reflecting bone turnover, mineralization kinetics and average bone matrix age. In contrast to BMD, which is an estimate of the total amount of mineral in a scanned area of whole bone, BMDD describes the local mineral content of the bone matrix throughout the sample. Moreover, the mineral content of the bone matrix is playing a pivotal role in tuning its stiffness, strength and toughness. BMDD of healthy individuals shows a remarkably small biological variance suggesting the existence of an evolutionary optimum with respect to its biomechanical performance. Hence, any deviations from normal BMDD due to either disease and/or treatment might be of significant biological and clinical relevance.

The development of appropriate methods to sensitively measure the BMDD in bone biopsies led to numerous applications of BMDD in the evaluation of diagnosis and treatment of bone diseases, while advancing the understanding of the bone material, concomitantly. For example, transiliacal bone biopsies of postmenopausal osteoporotic women were found to have mostly lower mineralization densities than normal, which were partly associated by an increase of bone turnover, but also caused by calcium and Vit-D deficiency. Antiresorptive therapy causes an increase of degree and homogeneity of mineralization within three years of treatment, while normal mineralization levels are not exceeded. In contrast, anabolic therapy like PTH decreases the degree and homogeneity of matrix mineralization, at least transiently. Osteogenesis imperfecta is generally associated with increased matrix mineralization contributing to the brittleness of bone in this disease, though bone turnover is usually increased suggesting an alteration in the mineralization kinetics. Furthermore, BMDD measurements combined with other scanning techniques like nanoindentation, Fourier transform infrared spectroscopy and small angle X-ray scattering can provide important insights into the structure–function relation of the bone matrix, and ultimately a better prediction of fracture risk in diseases, and after treatment.

© 2007 Elsevier Inc. All rights reserved.

**Keywords:** Bone mineralization density distribution; Quantitative backscattered electron imaging; Bone material quality; Hypermineralization; Hypomineralization

## Contents

Introduction . . . . .	457
Measuring BMDD . . . . .	457
Interpreting BMDD . . . . .	458
Sensitivity of BMDD analysis . . . . .	458
Normative reference BMDD . . . . .	460
Classification of deviations from normal mineralization density . . . . .	461
Hypermineralization and hypomineralization . . . . .	461
Shift towards high and low mineralization density . . . . .	461

\* Corresponding author. Fax: +43 1 91021 86929.

E-mail address: klaus.klaushofer@osteologie.at (K. Klaushofer).

BMDD from diseased and treated bone . . . . .	461
Osteoporosis and antiresorptive treatment . . . . .	461
Osteoporosis and calcium and vitamin D . . . . .	462
Osteoporosis and anabolic treatment . . . . .	462
Mild primary hyperparathyroidism . . . . .	462
Osteogenesis imperfecta . . . . .	462
Other bone diseases . . . . .	462
Bone phenotyping of experimental animals by BMDD . . . . .	462
Computer simulation of BMDD . . . . .	463
Combination with other methods. . . . .	464
Bone mineral density (BMD). . . . .	464
Other imaging techniques. . . . .	464
Outlook . . . . .	464
References . . . . .	464

## Introduction

Bone has a complex hierarchical structure, which is essential for its remarkable biomechanical performance. Bone strength is not only determined by bone mass, but also by geometry at the organ level, cortical and trabecular microarchitecture and intrinsic material properties. Thereby, the mineral content of the bone matrix is playing a pivotal role in tuning its stiffness, strength and toughness [1,2]. However, bone material is not homogeneous and isotropic. Human cortical and trabecular bones are formed by individual osteons and bone packets, respectively, sometimes called basic structural units (BSU) [3]. These BSUs are produced at different moments during the (re)modeling cycle by the coordinated activity of bone cells, whereby the osteoblasts synthesize, secrete and deposit the collagenous matrix, which then gradually mineralizes. Thus, each BSUs does not only have its own lamellar arrangement [4] of collagen fibrils but also a mineral content depending on the time since its deposition. This is the origin of a large local variation in material properties of bone [2,5,6].

Microradiography was the first technique to visualize and quantify the local variation in mineral content within cortices and trabeculae [7–11], showing that newly formed bone packets exhibit a lower mineral content. More advanced and sensitive techniques, such as quantitative backscattered electron imaging (qBEI) [12–18] and synchrotron radiation micro computed tomography (SR $\mu$ CT) [19,20] have been developed since then. For a quantitative analysis of micrometer scale variations in mineral content throughout the bone tissue, it is advantageous to use a histogram curve designated by us: *bone mineralization density distribution (BMDD)* [17,18]. BMDD is not a single value describing the mineral content but a histogram of mineral contents in small pixels or voxels within the area of investigation. Hence, BMDD is clearly different from bone mineral density (BMD) as measured by DXA (areal BMD, g/cm<sup>2</sup>) or qCT (volumetric BMD, g/cm<sup>3</sup>), which is an estimate of the total amount mineral in a scanned area of whole bone (organ level), but cannot distinguish local variations in mineral content (see for more details section *Combination with other methods*) [21–23].

The aim of this review is to summarize the present knowledge on BMDD from a technical or material science point of

view, then show its dependence on bone health and disease, and finally its development into a powerful tool for clinical applications. The method has applications in basic bone research and in bone phenotyping of genetically modified experimental animals. Complementary information on the bone matrix at identical topographic locations is obtained by combining qBEI with other scanning techniques, such as small angle and wide-angle X-ray scattering (SAXS/WAXS), nanoindentation (NI), scanning acoustic microscopy (SAM), Raman microspectroscopy (RAMAN) and Fourier transform infrared imaging (FTIRI). These combinations provide unique insights into questions of bone material quality and, more generally, into the structure–function relationship in mineralized tissues.

## Measuring BMDD

Quantitative microradiography (qMR), quantitative backscattered electron imaging (qBEI) and synchrotron radiation micro computed tomography (SR $\mu$ CT) may be utilized to measure distribution of mineral content in the form of the BMDD. All these methods require bone samples obtained by invasive techniques such as transiliac biopsies. However, block samples of undecalcified bone tissue prepared for histology and histomorphometry can be further used for the BMDD analysis. qMR [7,9–11] is based on unidirectional X-ray projection and absorption within 100  $\mu$ m thick bone sections resulting in the microradiograph which is analyzed [10,11] for its grey levels (having the meaning of mineral content in units of g/cm<sup>3</sup>). In contrast, qBEI [13–17] makes use of the fact that the intensity of electrons backscattered from a thin surface-layer (<1.5  $\mu$ m in thickness) of a sectioned bone area is proportional to the concentration of the bone mineral (wt.% calcium). The BMDD is derived from the digital images on a pixel basis. Our modification of the qBEI method is well established and validated [17]. Synchrotron radiation microtomography (SR $\mu$ CT) [19,20] is based on multidirectional projection and absorption of a focused, monochromatic X-ray beam by blocks of bone. The information obtained from the 3-dimensional measuring technique is combined with an imaging processing method that derives BMDD from analysis of voxels. The grey levels of

voxels represent mineral content in units of  $\text{g}/\text{cm}^3$ . Due to the long time needed for data acquisition and the huge amount of data to be handled, the analyzed volume is usually in the range of  $2 \times 2 \times 2 \text{ mm}^3$  at most. This method is rather new and still in development. There are also attempts to use normal (laboratory)  $\mu\text{CT}$  techniques to record BMDD [27]. However, X-ray fluxes in laboratory sources are such that a polychromatic beam has to be used, resulting in beam hardening effects, which are difficult to correct. Further, the signal to noise ratio is inferior compared to SR $\mu\text{CT}$ , reducing the capability to resolve differences in mineral contents.

As mentioned above the individual calibrated grey level pixels or voxels are reflecting the average mineral content found in the corresponding volume elements of the scanned sample region (Fig. 1). Thus, the acquisition of grey level pixel or voxel images provides the information of the local variation of mineral content throughout the bone tissue. This variation in mineral content is best described and quantified by a frequency distribution (histogram) of grey levels or mineral contents respectively (Fig. 2, BMDD). For statistical analysis and in order to compare different BMDDs with each other, a reduction of the huge amount of histogram data to only few characteristic parameters is necessary. For this purpose we introduced the parameters  $\text{Ca}_{\text{MEAN}}$  (the average calcium content in the bone volume of investigation),  $\text{Ca}_{\text{PEAK}}$  (the most frequent calcium content),  $\text{Ca}_{\text{WIDTH}}$  (the width of the calcium content distribution),  $\text{Ca}_{\text{LOW}}$  (the amount of lowly mineralized bone areas) and  $\text{Ca}_{\text{HIGH}}$  (the amount of highly mineralized bone areas) as described in Fig. 2. This method is found to be very efficient in quantifying differences between BMDD curves [24,28–30]. Another approach of BMDD evaluation was done, for example, by a reduction of the histogram to only a few bins by including multiple grey levels into one bin. Such an approach allows to compare BMDD curves on a bin-to-bin basis, by introducing

bins with very low, low, intermediate, high and very high mineral content [31–34].

## Interpreting BMDD

BMDD can be considered as a special attribute of bone reflecting bone turnover, mineralization kinetics and average tissue age. Two processes are responsible for the observed heterogeneity of bone matrix mineralization density in different bone packets (Fig. 2): 1) bone is continuously resorbed and newly formed during the bone (re)modeling process by bone multicellular units and 2) the newly deposited bone packets are mineralized following a certain not yet fully elucidated kinetic process of mineralization, which we started to investigate closer by *bone mineralization density profile (BM-profile)* analysis (Fig. 2). It could be shown that once mineralization has been started in the newly formed bone matrix (osteoid) the mineral content is rapidly increasing within a few days up to 70% of its final value [24–26]. This initial phase of mineralization typically referred as *primary mineralization* is followed by a slow phase of a gradual increase in mineral content in a time scale of years, called *secondary mineralization* (Fig. 2). This means that changes in bone turnover rates (resulting in the generation of altered amounts of new bone packets) as well as disturbances in mineralization kinetics will have a profound impact on the BMDD. Consequently, alterations in BMDD caused by diseases or treatments have to be interpreted with caution, taking into account both processes mentioned above. Therefore complementary information about bone turnover or existing mineralization abnormalities is needed for correct interpretation of the BMDD of an individual. Examples of BMDDs with different shape and peak positions are given in Fig. 4.

## Sensitivity of BMDD analysis

Crucial for sensitivity and quality of BMDD analysis is the reproducibility of BMDD acquisition and its resolution in mineral content. In our validated qBEI method [17] an inter-assay variance of 0.3% C.V. (coefficient of variance) for the mean Ca-content as opposed to 7% for the qMR method [8] was achieved. Instrumental stability, especially constant beam intensities, suitable calibration procedures by reference materials and minimizing the beam damage effects are required to maximize the resolution of differences in Ca-content, which is above all limited by the signal to noise ratio. The whole process of signal generation and detection underlies counting statistics inducing a broadening of BMDD peak which is less the better the signal to noise ratio is [35]. The validated qBEI method [17] is working with only a 5% peak broadening and a bin width resolution of 0.17wt.% Ca. (No data found for the other mentioned methods).

A second major problem is the voxel size compared to the typical feature size in the grey level analysis. Indeed, any voxel, which contains bone material, as well as bone marrow space (filled or not filled with embedding medium), will yield a wrong grey level. This is a potential problem for all the voxels at the bone surfaces. To get a rough feeling for this effect, we consider

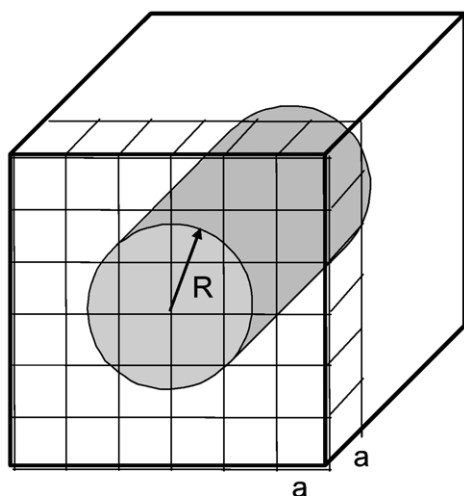


Fig. 1. Mineral content analysis by voxels. The grey levels of the voxels are reflecting the average mineral content in the corresponding sample volume element. The cylindrical bone structure with radius ( $R$ ) analyzed with a grid of voxels with edge length ( $a$ ) demonstrates that a fraction of voxels (depending on voxel size) are only partially filled with bone material yielding an artificially low value for mineral content.

a cylindrical structure viewed edge on (see Fig. 1). It is clear that all the voxels located close to the surface of the cylinder will only be partially filled with bone and, therefore, yield an artificially

low value for the calcium content. It is quite instructive to estimate the number of voxels affected in such a way in the example of Fig. 1. Calling  $R$  the radius of the cylinder and  $a$  the

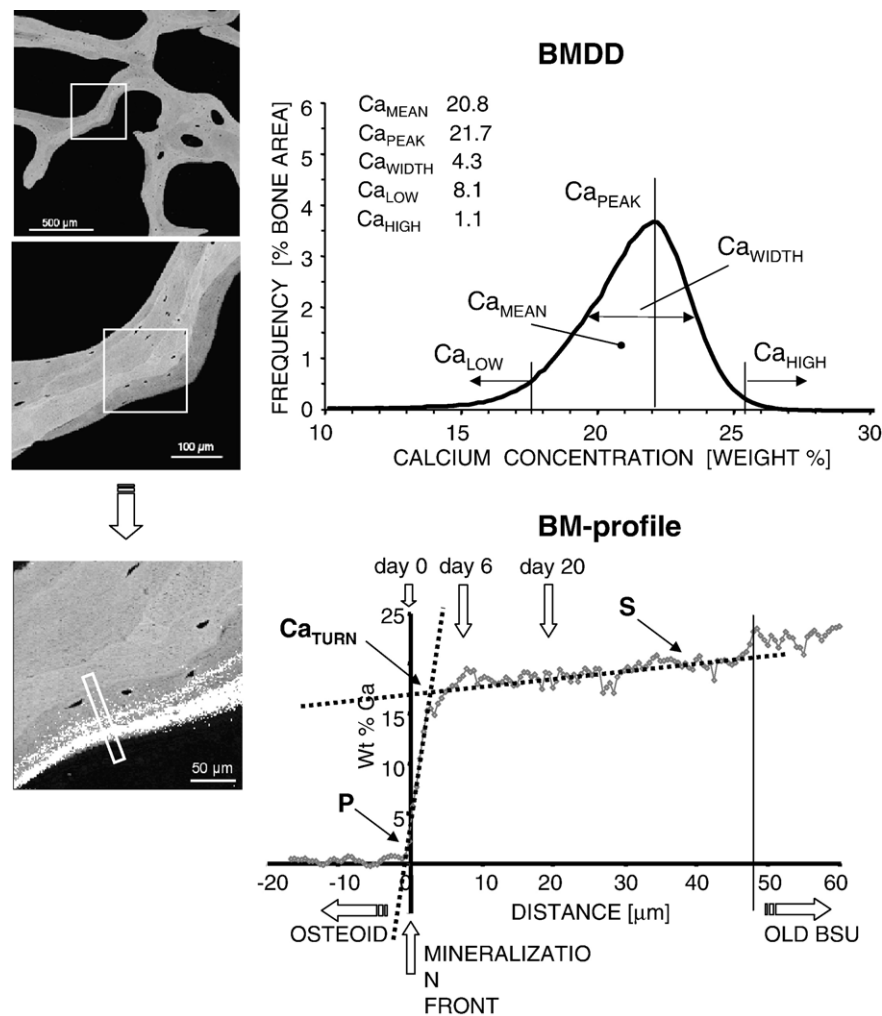
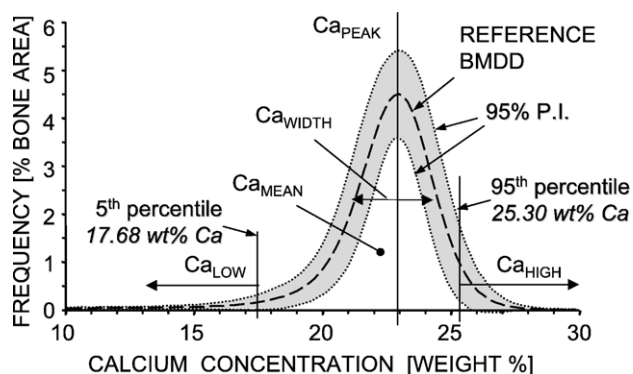


Fig. 2. Formation of bone mineralization density distribution (BMDD). Left side zoomed in series of backscattered electron (BE) images of trabecular bone. To be able to show the dynamics of mineralization a biopsy of a patient treated with PTH and double labeled with tetracycline was used [24]. Dark grey levels mean lower, bright grey levels higher mineral content and black soft tissue or resin. Upper image: overview to some trabecular features of transiliac biopsy; middle image: detail of upper image (rectangular white frame) showing the composition of trabeculae by individual bone packets of distinct mineral content. Lower image: detail of middle image (rectangular white frame) showing a new forming bone packet (dark grey) and fluorescence double labeling by tetracycline (visualized by white dots overlaid on the BE-images). Bar indicates the bone area where the line profile of calcium content were acquired shown in the diagram beside. Upper diagram: **BMDD** = bone mineralization density distribution corresponding BE-image; it is the grey level or calcium content frequency distribution of bone area scanned by quantitative backscattered electron imaging (qBEI) resulting from the contribution of all the bone packets. The histogram curve connects adjacent histogram data points. The x-axis indicates the Ca concentration (real, in multiples of the bin width) with a histogram bin width of 0.17 wt.% Ca, corresponding to one grey level step. The y-axis indicates the relative frequency of appearance of pixels having a certain Ca concentration given in percentage of mineralized bone area. The BMDD-parameters  $Ca_{MEAN}$ ,  $Ca_{PEAK}$ ,  $Ca_{WIDTH}$ ,  $Ca_{LOW}$ , and  $Ca_{HIGH}$ , characterizing the BMDD for statistical analysis are defined as:  $Ca_{MEAN}$ , the weighted mean Ca concentration of the bone area obtained from the integrated area under the BMDD curve in units of [wt.% Ca];  $Ca_{PEAK}$ , the peak position of the histogram, which indicates the most frequently measured calcium concentration (Ca value with the highest number of pixels) in the bone area in units of [wt.% Ca];  $Ca_{WIDTH}$ , the full width at half maximum of the distribution, describing the variation in mineralization density in units of [ $\Delta$ wt.% Ca] ( $\Delta$  = differences of Ca concentrations);  $Ca_{LOW}$ , the percentage of bone area that is mineralized below the 5th percentile of the reference range [18] in units [% bone area], that is below 17.68 wt.% Ca (see also Fig. 3), the parameter corresponds therefore also to the amount of bone area passing primary mineralization; and  $Ca_{HIGH}$ , the percentage of bone area that is mineralized above the 95th percentile of the reference range [18] in units [% bone area], that is above 25.30 wt.% Ca (see also Fig. 3), the parameter corresponds to the amount of bone area having achieved plateau level of mineralization (amount of fully mineralized bone matrix) and includes also the contribution of highly mineralized cement lines. (This parameter has been introduced here for the first time by the authors.) The lower diagram: **BM-profile** = bone mineralization profile of a newly forming bone packet; x-axis distance from the mineralizing front perpendicular into the depth of mineralized bone matrix (as indicated in the BE-image beside). The positions of fluorochrome labeling at day 20 and day 6 are marked by arrows. Day 0 means time of biopsy. y-axis is the Ca-content values measured in steps of 0.5 μm into the bone matrix. The profile can be fitted by two linear regression lines with an initial steep slope ( $P$ ) for primary mineralization and a flat slope ( $S$ ) for secondary mineralization indicating a fast followed by a slow process of mineralization. Both lines are crossing at the point designated by us as  $Ca_{TURN}$ , the Ca-content, where the transition from fast to slow mineralization is occurring. (This additional evaluations of mineralization profiles are unpublished data.)



BMDD-parameter	mean $\pm$ SD
Ca <sub>MEAN</sub> [wt% Ca]	22.20 $\pm$ 0.45
Ca <sub>PEAK</sub> [wt% Ca]	22.94 $\pm$ 0.39
Ca <sub>WIDTH</sub> [ $\Delta$ wt% Ca]	3.35 $\pm$ 0.34
Ca <sub>LOW</sub> [% bone area]	4.93 $\pm$ 1.57
Ca <sub>HIGH</sub> [% bone area]	5.55 $\pm$ 3.32

Fig. 3. Normative reference BMDD for trabecular bone of adults. Dashed line with short lines: indicates mean BMDD generated from histogram data of 52 individuals including various biological factors like, gender, age, ethnic, origin and skeletal sites [18]. Dashed lines with points: indicate border of the prediction interval (P.I.) to find 95% of the data within it (grey area). For the definition of the BMDD-parameters Ca<sub>MEAN</sub>, Ca<sub>PEAK</sub>, Ca<sub>WIDTH</sub>, Ca<sub>LOW</sub>, Ca<sub>HIGH</sub> see figure legend of Fig. 2.

edge length of the voxel, the fraction of wrong grey levels will be roughly  $f \approx 2\pi Ra / \pi R^2 \approx 2a/R$ . Taking  $R \approx 100 \mu\text{m}$  for a typical feature size in cancellous bone (where the thickness of trabeculae is in the order of  $200 \mu\text{m}$ ), the fraction of bad voxels in the BMDD curve will be in the order of 2% for a voxel size of  $1 \mu\text{m}$ . For a voxel size of  $10 \mu\text{m}$ , the number of bad voxels will already be in the order of 20% and when the voxel resolution gets lower, the BMDD curve becomes essentially meaningless, at least in cancellous bone. In cortical bone, the situation is less dramatic as there are fewer interfaces (mostly only Haversian canals). It is

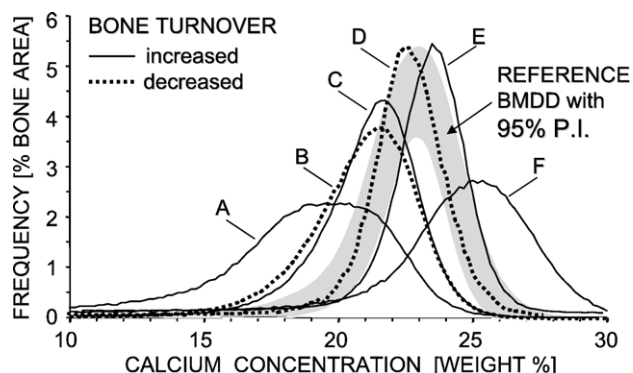


Fig. 4. BMDDs of healthy and diseased or treated bone. Examples of variations in BMDDs from transiliac biopsies as a result of different bone turnover and/or mineralization kinetics. A: osteomalacia (coeliac disease), B: idiopathic osteoporosis, C: postmenopausal osteoporosis, D: postmenopausal osteoporosis treated with bisphosphonates, E: osteogenesis imperfecta type I of a child, F: postmenopausal osteoporosis treated with NaF. Reference BMDD [18]: see also Fig. 3; see Table 1 for the corresponding values of deviations from normative reference BMDD-parameters.

worth mentioning that the different measuring techniques are quite different in terms of their voxel resolution. qMR requires specimens of about  $100 \mu\text{m}$  thickness which are measured in transmission. According to the simple estimate above, this means that this technique does not provide meaningful BMDD data for cancellous bone and its application should be restricted to cortical bone. SR $\mu$ CT can be used with a voxel size of  $5 \mu\text{m}$  or even better and is well suited also for cancellous bone. The difficulty here is to avoid artifacts in the three-dimensional reconstruction, but there is rapid progress in this field. Voxel resolution is not a problem for qBEI, as the sampling depth of electrons backscattered from the surface of the bone specimen is only of  $1\text{--}1.5 \mu\text{m}$ . In this sense, qBEI is truly two-dimensional and grey level artifacts of the type discussed above would only appear if the lateral resolution were chosen much larger than, say  $5 \mu\text{m}$ . Typically, we take a pixel size of  $(1\text{--}4 \mu\text{m})$ .

### Normative reference BMDD

In order to estimate the biological variance of BMDD, a systematic analysis of the influences of various biological factors on the BMDD in normal (healthy) bone was performed by us using the qBEI method [18]. Trabecular bone of different skeletal sites (transiliac bone, vertebrae, femoral neck and head, patella) from adult individuals (age 25–90 years), of different ethnicity (African and Caucasian Americans) and gender were analyzed. The surprising outcome was that none of these biological factors caused significant differences within the corresponding sample groups [18]. Consistently, an analysis of age dependency in normal transiliac biopsies using the qMR method [11] did not show significant changes in BMDD either. Thus, a general reference BMDD of human adult trabecular bone including 52 individual BMDDs with varying aspects of biological factors could be established and normative BMDD-parameters calculated (Fig. 3). In comparison to other biological variables, the BMDD showed rather small variations (the coefficient of variance for Ca<sub>MEAN</sub> was only 2.1%). As a result, the normal BMDD was deemed to be “constant” [18] and already small deviations in BMDD induced by metabolic bone diseases or treatments could be detected. The need of only one general reference BMDD is a big advantage in using the BMDD as a diagnostic tool or in monitoring treatment compliance. Based on our experience thus far, there seems to be no need for separate normal reference sample collection for each biological factor (e.g. skeletal site, age, sex) or their combination, which would be difficult to establish in many cases, but could be done if necessary.

Table 1

Percent deviations from normative reference BMDD-parameters for the examples of diseased or treated bone corresponding to BMDDs of Fig. 4

Patient	$\Delta$ Ca <sub>MEAN</sub> [%]	$\Delta$ Ca <sub>PEAK</sub> [%]	$\Delta$ Ca <sub>WIDTH</sub> [%]	$\Delta$ Ca <sub>LOW</sub> [%]	$\Delta$ Ca <sub>HIGH</sub> [%]
A	−19	−14	+92	+628	−97
B	−7	−7	+19	+86	−87
C	−6	−6	+7	+93	−86
D	+2	+1	−12	−29	−28
E	+2	+3	−12	+10	+61
F	+2	+10	+50	+190	+634

Considering the rather small biological variations in the BMDD of adult trabecular bone, the BMDDs may reflect an evolutionary optimum in bone matrix mineralization density as a result of bone cells activity and mechanical loading, resulting in an optimum combination between stiffness and toughness of the bone material [36]. Hence, significant differences from the normative data are most likely of biological relevance e.g. the decreased or increased mineralization density found in osteoporosis [37] or the increased mineralization in osteogenesis imperfecta (Fig. 4) [32,38].

### Classification of deviations from normal mineralization density

In order to classify the deviation of mineralization density from that of normal, it is useful to distinguish between the different structural levels of bone and define the nomenclature used. We therefore suggest the following nomenclature (examples will be given in the course of this review).

#### *Hypermineralization and hypomineralization*

Mineralization density at the bone matrix level of mature lamellar bone, the level of individual bone packets (a single BSU), is characterized by its mean mineral content. During secondary mineralization, the mineral content of an individual bone packet continuously increases with time (mineralization law). There is evidence that free water in the matrix is gradually replaced by mineral and that the mineralization density is, thus, slowly approaching a plateau value corresponding to saturation with mineral [2,39,40]. qBEI measurements of the most highly mineralized bone matrix regions in our sample collective revealed a plateau value around 25.3 wt.% Ca, which coincides with the Ca-content value of the 95th percentile of the normative reference BMDD. These highly mineralized bone regions usually correspond to interstitial bone, most likely residuals of old bone packets left over in the remodeling process. Cement-lines, which are bordering the bone packets and can even be more highly mineralized, were excluded from these evaluations. Consequently, we suggest defining *hypermineralization* and *hypomineralization* as deviations from mineral content of such fully mineralized bone matrix. Thus, only a pathologically altered organic matrix and/or abnormalities in crystal size and shape can lead to a hypermineralization, a mineralization density exceeding that of fully mineralized normal bone matrix. In contrast, in the case of hypomineralization the organic matrix is not fully mineralized due to lack of time for secondary mineralization and/or by pathologically altered bone matrix affecting normal mineralization kinetics.

#### *Shift towards high and low mineralization density*

The mineralization density at the tissue level, reflecting the contribution of all BSUs with different degrees of mineralization, is characterized by the resulting BMDD. A BMDD with a higher  $Ca_{MEAN}$  and  $Ca_{PEAK}$  than normal reference BMDD will be designated as a BMDD with a *shift to high mineralization density* and a BMDD with lower  $Ca_{MEAN}$  and  $Ca_{PEAK}$  than

normal as a BMDD with a *shift to low mineralization density*. For BMDDs with broader or narrower peaks than normal the terms *more heterogeneous* or *more homogeneous*, respectively are suggested. Diseases with BMDD shifts to high mineralization density may be due to a hypermineralization of an altered bone matrix or just an increased amount of higher or fully mineralized bone packets caused by low turnover for instance. In contrast, a disease with BMDD shifts to low mineralization density results from an abnormally high amount of lower mineralized bone packets usually due to increased bone turnover. However, if the mineralization kinetics is also altered then even the contrary is plausible. This seems to be the case for instance in osteogenesis imperfecta, where bone turnover is high, but mineralization kinetics are likely to be accelerated, or idiopathic osteoporosis, where bone turnover is low, but the mineralization kinetic is likely to be decelerated (Fig. 4).

### BMDD from diseased and treated bone

#### *Osteoporosis and antiresorptive treatment*

For the most part, BMDD measurements were performed on bone biopsies from clinical trials of osteoporosis for monitoring and testing the effects of the treatment, or on bone samples from animal models. The typical effect on the BMDD as we found using our qBEI method [18] was a characteristic reduction in the peak width ( $Ca_{WIDTH}$ ) of the distribution and a slight shift of the peak position towards higher mineral content (Fig. 4) after an antiresorptive treatment for two or three years (or analogous duration in animal trials). This was first observed in a minipig animal model [41] as well as in postmenopausal osteoporotic women treated with alendronate [42] and in the VertNA-study after 3 years of risedronate [28]. Comparable effects on BMDD were found also with zoledronate in renal osteodystrophy [43] and after liver transplantation [44]. Furthermore, in an aged rat model of osteopenia, treatment with OPG as an antiresorptive agent also resulted in narrowing of the BMDD [45]. Consistently, the SR $\mu$ CT method applied in the VertNA-study revealed comparable effects on BMDD [20]. In the case of the alendronate study qMR [46] also detected the increase in mean degree of mineralization, but not the change in peak width. Further, qMR observed similar effects on BMDD after estrogen, and Raloxifen treatments [47,48]. These effects on BMDD are likely due to the rapid and sustained antiresorptive action and reduction in bone turnover. Already formed bone packets continue to mineralize while fewer new bone packets are generated, resulting in less bone in the primary mineralization stage (lower mineral content) and more bone in the prolonged secondary mineralization stage (higher and more homogeneous mineral content). Surprisingly, the narrowing of the BMDD was observed to be transient, since after 5 years of alendronate or risedronate treatment, the BMDD was found to come back to normal width, suggesting that bone turnover has reached a new equilibrium state after 5 years of treatment. The transient narrowing of the BMDD within the first 3 years of antiresorptive treatment is also consistent with the results of mathematical modeling of the BMDD curve [49].

### *Osteoporosis and calcium and vitamin D*

The postmenopausal osteoporosis placebo group in the alendronate trial exhibited a distinct BMDD shift to low mineralization density combined with an increased peak width compared to normal (Fig. 4) [42]. The same was observed for both the placebo and the treatment groups at baseline in the risedronate study [28], which was found to be associated with an increased bone turnover rate as measured by histomorphometry. Since this was a paired/triplet biopsy study for both groups, the effect of calcium & Vit-D could be separated from that of risedronate. Interestingly, calcium & Vit-D supplementation as given in the study protocol already resulted in a BMDD shift back towards normal mineralization density, albeit without reducing the BMDD peak width. Further analysis of the bone samples from the risedronate study [23] revealed that the positive effect of calcium & Vit-D on the mineral content (increase) was proportional to the deficiency in mineralization density at baseline. Such a beneficial effect of calcium & Vit-D on the mean degree of mineralization was observed also in the Raloxifen study using qMR [48].

### *Osteoporosis and anabolic treatment*

NaF in a dosage of 60mg/day has been used in several European countries for osteoporosis treatment. Bone formation and BMD were found to be dramatically increased in treated patients, however, no antifracture efficacy of this treatment could be proven [50]. qBEI analysis combined with SAXS measurements clearly demonstrated that the bone matrix formed in presence of NaF had altered nanocomposite properties [51]. The matrix was hypermineralized (Fig. 4) and the mineral particle size distribution completely changed, with the presence of abnormal, big mineral crystals. Consequently, the large amount of newly formed bone was of bad quality and this explains why no improvement of the mechanical competence of NaF-treated bone could be observed despite the increase of BMD [50]. Intermittent treatment with PTH is now approved for anabolic treatment worldwide. This treatment caused the BMDD to shift slightly to lower mineralization densities with an increased peak width due to the increased formation of new bone matrix [24]. In an estrogen-depleted rat animal model comparable effects on BMDD could be observed [52]. It can be assumed, that this effect is only transient and if PTH therapy would be followed by an antiresorptive treatment the matrix would have time for a longer period of secondary mineralization and the BMDD would normalize eventually.

### *Mild primary hyperparathyroidism*

Mild primary hyperparathyroidism (pPTH) is characterized by abnormally elevated PTH serum levels accompanied by asymptomatic hypercalcemia. Typically, the BMDDs were found to be shifted towards lower mineralization density (Fig. 4) [30]. Combined histomorphometry and qBEI analysis of biopsies revealed a highly linear correlation between the mineralizing surface (MS/BS) and all four BMDD-parameters. For  $Ca_{MEAN}$

and  $Ca_{PEAK}$  the correlation was negative and for  $Ca_{WIDTH}$  and  $Ca_{LOW}$  positive. These findings fully confirm the concept of interpretation of the BMDD as described before. Since there is no evidence of any change in the kinetics of mineralization in pHPT the observed changes in BMDD can be interpreted exclusively as the result of the increased bone turnover and bone formation rate. These results confirmed those obtained earlier by qMR [25].

### *Osteogenesis imperfecta*

Osteogenesis imperfecta (OI) is a genetic disorder with increased bone fragility. In the majority of patients, mutations affecting collagen type I can be attributed to the typical OI phenotype [53]. All studies on BMDD to date showed a shift towards a higher mineralization density of bone tissue, only marginally exceeding that of normal adults (Fig. 4) [32,38]. It seems at least in mild OI that the shift in BMDD to higher mineral content is not based exclusively on an altered collagen structure, but might be also caused by an accelerated mineralization process [38]. Studies in the oim mouse model of OI including mechanical and material properties confirmed the typical increased mineralization density [54]. The findings gave a picture of pathologically altered material properties contributing to the increased hardness and brittleness of the OI bone [55,56]. Further BMDD measurements on treated OI bone helped to understand why bisphosphonates therapy unexpectedly could decrease fracture incidence in OI children and in OI mouse model animals (oim). In bone from both pamidronate treated OI children and also from alendronate oim, the bisphosphonates did not cause any additional changes of the material properties, but lead to a general increase in volume and especially cortical thickness of growing bone [38,57].

### **Other bone diseases**

Alterations in the BMDD have also been measured in male osteoporosis, idiopathic osteoporosis, patients with collagen I polymorphisms [29], osteomalacia [18], hypophosphatemia, Paget's disease, Bruck's Syndrome, myopathy, renal osteodystrophy [43], and liver transplantation [44]. All of them showed a distinct BMDD shift to lower mineralization density (e.g. Fig. 4), while pycnodysostosis [58], hypoparathyroidism, osteopetrosis, and osteonecrosis exhibited a tendency to a BMDD shift to higher mineralization density. Furthermore, a decreased mineral content of the osteoporotic femoral neck could be associated with bone fragility of the hip [31].

### **Bone phenotyping of experimental animals by BMDD**

Experimental animal models with defined genetic modifications are of particular importance for bone research. On one hand they open new insight in osteogenesis, processes of mineralization, production of bone matrix, bone metabolism, regulation of osteoblasts and osteoclasts, generation of special bone phenotypes, etc. On the other hand they enable completely new possibilities to study the structure–function relations of the bone material and how it is deteriorated by diseases. Additionally,

animal models help to develop new treatment strategies targeting the specific defect of the disease.

As already described before, the oim mouse model enabled to study the characteristic alterations of human OI bone [54–57]. A transgenic mouse with targeted overexpression of the vitamin D receptor (VDR) in osteoblasts, revealed an overexpression dependent shift of the BMDD towards higher mineralization density of 3.14% and 3.34%, respectively [59]. Tissue non-specific alkaline phosphatase (TNALP) deficient mice displayed a retarded mineralization with a highly heterogeneous mineralization pattern [60]. Interestingly, mice overexpressing Fra-1 showed a bone phenotype with an increased bone volume, while the bone material quality seemed to be preserved [61]. The

BMDD displayed only a small shift towards lower mineralization in these growing animals and nanocomposite structure as measured by SAXS was unchanged. In contrast, the C-fos knock out mice lacking osteoclasts had a BMDD shift towards high mineralization density caused mainly by highly mineralized cartilage (hypomineralization) not being resorbed by the osteoclasts [61].

### Computer simulation of BMDD

A mathematical model for computer simulation of the BMDD was established [49], which is based on the two processes occurring in bone tissue: a) the deposition and the resorption of bone

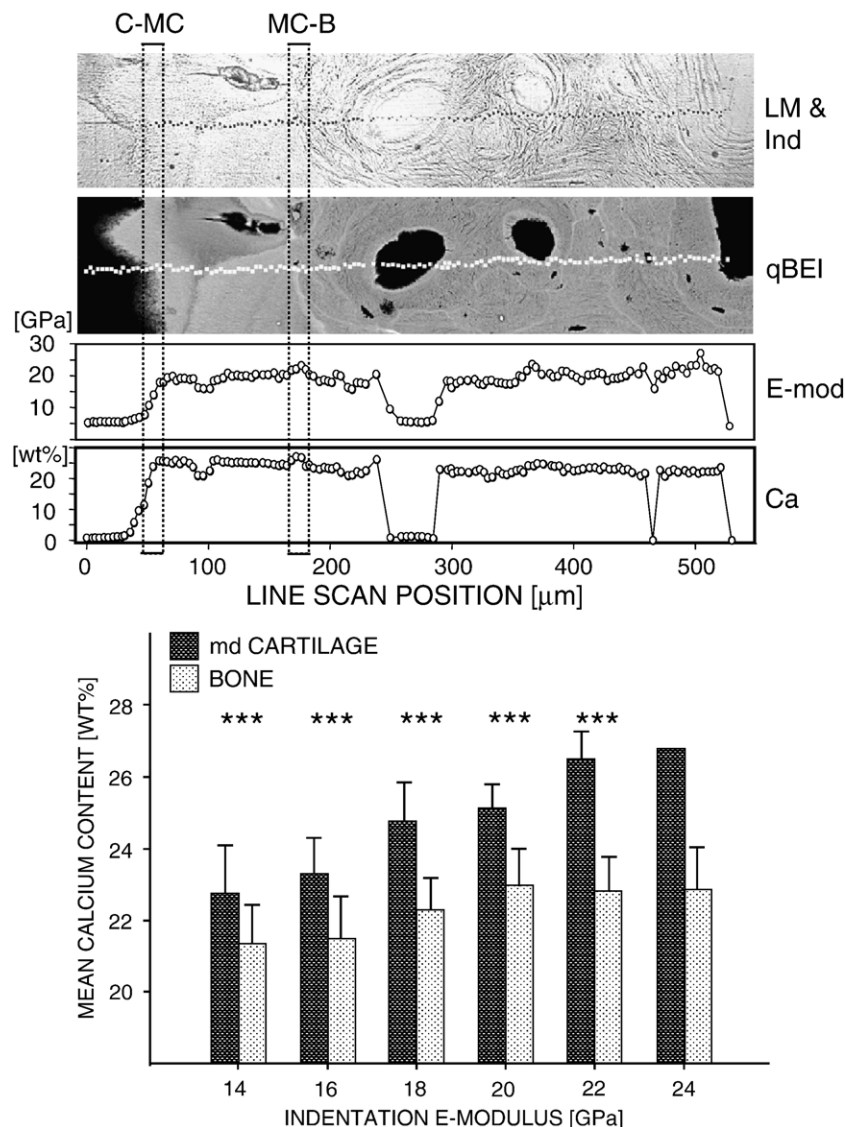


Fig. 5. Combination of nanoindentation with qBEI/BMDD. Tissue section of human patella containing articular cartilage and subchondral bone was studied by nanoindentation and qBEI to gain information about intrinsic material properties [69]. The upper image (LM & Ind) shows a reflected light microscopical image taken after nanoindentation. The indents of the indentation line scan are visible as black dots. Second image (qBEI) visualizes the mineralized part of the tissue. C-MC = transition of articular cartilage from non-mineralized to mineralized matrix (tide mark); MC-B = transition from mineralized cartilage to subchondral bone. White marks indicating the positions, identical with that of nanoindentation, where the local mean calcium content was determined. Diagram (*E-mod*) displays E-modulus data of the line scan. Diagram (*Ca*) shows the corresponding Ca-content data. It is clearly visible that the E-modulus is directly related to the Ca-content. The bar diagram below summarizes another striking result from this combined study: the matrix of cartilage needs a much higher mineral content to achieve a similar stiffness (E-modulus) than the bone matrix.

matrix described by the bone turnover rate and b) the kinetics of matrix mineralization (mineralization law). For a first approach a quasi-stationary state in BMDD has been considered. Applying the model on the experimental measured BMDD two interesting results could be obtained: first, a two-phase mineralization process with a fast primary phase and about three orders slower secondary phase is needed to receive a peaked BMDD as seen in Fig. 2. Second, the turnover rate of the remodeling process has a strong influence on the peak position ( $Ca_{PEAK}$ ) and the shape of the BMDD. Higher turnover rates caused BMDD shifts to low mineralization density and vice versa, consistent with experimentally measured BMDDs (Fig. 4). Generally, computed modeling of the BMDD offers new possibilities for the analysis and interpretation of the experimentally measured BMDD altered by diseases and treatments. Further, it could help to select and develop therapeutic strategies directly targeting the underlying defects of the disease with the aim to bring the BMDD back to normal.

### Combination with other methods

#### *Bone mineral density (BMD)*

BMD (areal BMD) as measured by DXA is, in fact, a composite variable influenced by bone volume, bone size and bone matrix mineralization density. It could be shown that the combination of BMD and BMDD measurements allows distinguishing between effects on bone volume and degree of mineralization, which is of important clinical interest for treatment evaluation. Using a combined data set from the VertNA risedronate study of BMD from the spine and of BMDD from transiliac biopsy before and after treatment following interesting results were observed: i) the about 8% increase of BMD found in risedronate treated group (risedronate plus calcium & Vit-D) was mainly caused by an intrinsic increase ( $\sim 5\%$ ) in mineral content of the bone matrix, while the bone volume was essentially preserved. ii) the unchanged BMD as found in the placebo treated group (calcium & Vit-D) was the result of an about 3.5% increase in mineral content and a simultaneous drop in bone volume of about 3.5% [23].

#### *Other imaging techniques*

As an imaging tool, qBEI can advantageously be combined with other imaging techniques, which give information other than mineral content. Scanning small angle X-ray scattering, (SAXS) is an example for such a method, which gives information on the size, shape, arrangement and orientation of mineral particles [62–64]. This allows a simultaneous analysis of the amount of mineral (qBEI) and the size of mineral crystals (SAXS) in the same tissue, e.g. during bone development in humans [65] or animals [66], or at the bone–cartilage interface [67]. The same combination has also proven to be useful in examining changes in bone material quality after osteoporosis treatments like NaF, alendronate, intermittent PTH, OPG or diseases like osteogenesis imperfecta and pycnodysostosis [51,42,24,46,55,56,58].

Recently, qBEI/BMDD has also been shown to be an important parameter for the interpretation of mechanical deformation tests

such as nanoindentation experiments (Fig. 5) [5,36,68,69] tensile tests [70–72] or crack propagation experiments [73]. Generally, the E-modulus showed a non-linear positive relationship with the mineral content and a strong dependency on the mechanical properties (shear modulus) of the organic matrix.

Lately, Fourier transform infrared imaging (FTIRI) has been developed to analyze the spatial distribution of collagen cross linking like the  $P_{\text{ry}}/deH\text{-DHLNL}$  ratio which is thought to play an important role in the mechanical performance of the bone tissue [74]. The combination of qBEI and FTIRI gives evidence that in general the bone matrix with higher mineral content also exhibited a higher  $P_{\text{ry}}/deH\text{-DHLNL}$  ratio indicative of its higher tissue age. Furthermore, FTIRI line scans through forming bone packets of normal, untreated osteoporotic and risedronate treated bone showed differential effects in collagen cross linking pattern within the first 50  $\mu\text{m}$  in depth of the bone packet [75].

### Outlook

There are already numerous, successful applications of BMDD in the evaluation of diagnosis and treatment of bone diseases. This was coupled with progress in the basic understanding of the bone material and of the mechanisms leading to a BMDD curve with a specific shape. Indeed, two processes were found to play a major role in defining the shape of this curve: the first is bone turnover, which could be clearly demonstrated by correlations of BMDD with dynamic histomorphometry and by mathematical simulation. The second is the kinetics of matrix mineralization, which still needs to be studied more extensively.

Until now we have introduced a normative reference BMDD only for the trabecular bone compartment of adults. Since many of the bone disorders are affecting children, it would be important to establish analogous normative BMDD references data covering the age range from birth to adolescence. Further, normative data for BMDD of cortical bone, which comprises 75% of the bone mass and is the most load-bearing bone compartment, would also be of important clinical value. Moreover, the expansion of the mathematical model of BMDD to non-stationary scenarios will allow to simulate transient changes in bone turnover, bone volume and mineralization law and thus to predict outcomes of BMDD by different treatments regimes.

New combinations of qBEI with other scanning techniques such as Raman microspectroscopy [6,76] and scanning acoustic microscopy [77] will allow the analysis of the chemical properties of the corresponding organic matrix and the elastic properties of the corresponding sites. Such a set of site-matched complementary data would give important insights to the structure function relation of the bone matrix, and ultimately a better prediction of fracture risk in diseases and after treatment.

### References

- [1] Currey JD. Bones: structure and mechanics. Princeton, NJ: Princeton Univ. Press; 2002. p. 436.
- [2] Fratzl P, Gupta HS, Paschalis EP, Roschger P. Structure and mechanical quality of the collagen-mineral nano-composite in bone. *J Mater Chem* 2004;14:2115–23 Review.

- [3] Eriksen EF, Axelrod DW, Melsen F. Bone histomorphometry. New York: Raven Press; 1994.
- [4] Weiner S, Traub W, Wagner HD. Lamellar bone: structure–function relations. *J Struct Biol* 1999;126:241–55.
- [5] Gupta HS, Stachewicz U, Wagermaier W, Roschger P, Wagner HD, Fratzl P. Mechanical modulation at the lamellar level in osteonal bone. *J Mater Res* 2006;21:1913–21.
- [6] Kazanci M, Wagner HD, Manjubala NI, Gupta HS, Paschalis EP, Roschger P, et al. Raman imaging of two orthogonal planes within cortical bone. *Bone* 2007;41:456–61.
- [7] Ambrino E, Engstrom A. Studies on X-ray absorptions and diffraction of bone tissues. *Acta Anat* 1952;15:1–22.
- [8] Jowsey J. Variations in bone mineralization with age and disease. In: Frost HM, editor. *Bone biodynamics*. Boston, MA: Little, Brown & Company; 1964. p. 461–79.
- [9] Bovin G, Baud CA. Microradiographic methods for calcified tissues. In: Dickson GR, editor. *Methods for calcified tissue preparation*. Amsterdam: Elsevier Science Publishers; 1984. p. 391–411.
- [10] Eschberger J, Eschberger DJ. Microradiography. In: von Recum FA, editor. *Handbook of biomaterials evaluation*. New York: Macmillan Publishing Company; 1986. p. 491–500.
- [11] Boivin G, Meunier PJ. The degree of mineralization of bone tissue measured by computerized quantitative contact microradiography. *Calcif Tissue Int* 2002;70:503–11.
- [12] Boyde A, Jones SJ. Backscattered electron imaging of skeletal tissues. *Metab Bone Dis Rel Res* 1983;5:145–50.
- [13] Reid SA, Boyde A. Changes in the mineral density distribution in human bone with age: image analysis using backscattered electrons in SEM. *J Bone Miner Res* 1987;2:13–22.
- [14] Skedros JG, Bloebaum RD, Bachus KN, Boyce TM, Constantz B. Influence of mineral content and composition on gray levels in backscattered electron images of bone. *J Biomed Mater Res* 1993;27:57.
- [15] Bloebaum RD, Skedros JG, Vajda EG, Bachus KN, Constantz BR. Determining mineral content variations in bone using backscattered electron imaging. *Bone* 1997;20:485–90.
- [16] Roschger P, Plenck Jr H, Klaushofer K, Eschberger J. A new scanning electron microscopy approach to the quantification of bone mineral distribution: backscattered electron image grey-levels correlated to calcium Ka-line intensities. *Scanning Microsc* 1995;9:75–88.
- [17] Roschger P, Fratzl P, Eschberger J, Klaushofer K. Validation of quantitative backscattered electron imaging for the measurement of mineral density distribution in human bone biopsies. *Bone* 1998;23:319–26.
- [18] Roschger P, Gupta HS, Berzlanovich A, Ittner G, Dempster DW, Fratzl P, et al. Constant mineralization density distribution in cancellous human bone. *Bone* 2003;32(3):316–23.
- [19] Nuzzo S, Lafage-Proust MH, Martin-Badosa E, Boivin G, Thomas T, Alexandre C, et al. Synchrotron radiation microtomography allows the analysis of three-dimensional microarchitecture and degree of mineralization of human iliac crest biopsy specimens: effects of edidronate treatment. *J Bone Miner Res* 2002;17:1372–82.
- [20] Borah B, Ritman EL, Dufresne TE, Jorgensen SM, Liu S, Sacha J, et al. The effect of risedronate on bone mineralization as measured by micro-computed tomography with synchrotron radiation: correlation to histomorphometric indices of turnover. *Bone* 2005;37:1–9.
- [21] Miller PD, McClung M. Prediction of fracture risk. I: bone density. *Am J Med Sci* 1996;312:257–9.
- [22] Meunier PJ, Boivin G. Bone mineral density reflects bone mass but also the degree of mineralization of bone: therapeutic implications. *Bone* 1997;21(5):373–7.
- [23] Fratzl P, Roschger P, Fratzl-Zelman N, Paschalis EP, Phipps R, Klaushofer K. Evidence that treatment with risedronate in women with postmenopausal osteoporosis effects bone mineralization and bone volume. *Calcif Tissue Int* 2007;81(2):73–80.
- [24] Misof BM, Roschger P, Cosman F, Kurland ES, Tesch W, Messmer P, et al. Effects of intermittent parathyroid hormone administration on bone mineralization density in iliac crest biopsies from patients with osteoporosis: a paired study before and after treatment. *J Clin Endocrinol Metab* 2003;88(3):1150–6.
- [25] Boivin G, Meunier PJ. Changes in bone remodeling rate influence the degree of mineralization of bone. *Connect Tissue Res* 2002;43(2–3):535–7.
- [26] Boivin G, Meunier PJ. Methodological considerations in measurement of bone mineral content. *Osteoporos Int* 2003;14:S22–7.
- [27] Mulder L, Koolstra JM, van Eijden TGMJ. Accuracy of microCT in the quantitative determination of the degree and distribution of mineralization in developing bone. *Acta Radiol* 2004;45:769–77.
- [28] Zoehrer R, Roschger P, Durchschlag E, Fratzl P, Paschalis E, Recker R, et al. Bone mineralization density distribution in triple biopsies of the iliac crest in post-menopausal women. *J Bone Miner Res* 2006;21(7):1106–12.
- [29] Stewart, Roschger P, Misof BM, Mann V, Fratzl P, Klaushofer, et al. COL1A1Sp1 alleles are associated with defective bone mineralization in vivo and in vitro. *Calcif Tissue Int* 2004;77:113–8.
- [30] Roschger P, Dempster DW, Zhou H, Paschalis EP, Silverberg SJ, Shane E, et al. New observations on bone quality in mild hyperparathyroidism as determined by quantitative backscattered electron imaging. *J Bone Miner Res* 2007;22:717–23.
- [31] Loveridge N, Power J, Reeve J, Boyde A. Bone mineralization density and femoral neck fragility. *Bone* 2004;35(4):929–41.
- [32] Boyde A, Travers R, Glorieux FH, Jones SJ. The mineralization density of iliac crest bone from children with osteogenesis imperfecta. *Calcif Tissue Int* 1999;64:185–90.
- [33] Boyde A, Compston JE, Reeve J, Bell KL, Nobel BS, JHones SJ, et al. Effect of estrogen suppression on the mineralization density of iliac crest biopsies in young women as assessed by backscattered electron imaging. *Bone* 1998;22:241–50.
- [34] Boyde A, Jones SJ, Aerssens J, Dequeker J. Mineral density quantitation of the human cortical iliac crest by backscattered electron image analysis. Variations with age, sex, and degree of osteoarthritis. *Bone* 1995;16: 619–27.
- [35] Roschger P, Fratzl P, Eschberger J, Klaushofer K. Response to the letter to the editor by E.G. Vajda and J.G. Skedros. *Bone* 1999;24(6):620–1.
- [36] Turner CH. Biomechanics of bone: determinants of skeletal fragility and bone quality. *Osteoporos Int* 2002;13(2):97–104 Review.
- [37] Ciarelli TE, Fyhrie DP, Parfitt AM. Effects of vertebral bone fragility and bone formation rate on the mineralization level of cancellous bone from white females. *Bone* 2003;32:311–5.
- [38] Weber M, Roschger P, Fratzl-Zelman N, Schöberl T, Rauch F, Glorieux FH, et al. Pamidronate does not adversely affect bone intrinsic material properties in children with osteogenesis imperfecta. *Bone* 2006;39: 616–22.
- [39] Jaeger I, Fratzl P. Mineralized collagen fibrils: a mechanical model with a staggered arrangement of mineral particles. *Biophys J* 2000;79(4):1737–46.
- [40] Fratzl P, Fratzl-Zelman N, Klaushofer K. Collagen packing and mineralization: an X-ray scattering investigation of turkey leg tendon. *Biophys J* 1993;64:260–6.
- [41] Roschger P, Fratzl P, Klaushofer K, Rodan G. Mineralization of cancellous bone after alendronate and sodium fluoride treatment: a quantitative backscattered electron imaging study on minipig ribs. *Bone* 1997;20: 393–7.
- [42] Roschger P, Rinnerthaler S, Yates J, Rodan GA, Fratzl P, Klaushofer K. Alendronate increases degree and uniformity of mineralization in cancellous bone and decreases the porosity in cortical bone of osteoporotic women. *Bone* 2001;29(2):185–91.
- [43] Haas M, Leko-Mohr Z, Roschger P, Kletzmayer J, Schwarz C, Mitterbauer C, et al. Zoledronic acid to prevent bone loss in the first six months after renal transplantation. *Kidney Int* 2003;63:1130–6.
- [44] Bodingbauer M, Wekerle T, Pakrah B, Silberhumer G, Roschger P, Peck-Radosavljevic M, et al. Prophylactic bisphosphonate treatment prevents bone fractures after liver transplantation. *Am J Transplant* 2007;7 (7):1763–9.
- [45] Valenta A, Roschger P, Fratzl-Zelman N, Kostenuik JP, Dunstan CR, Fratzl P, et al. Combined treatment with PTH (1–34) and OPG increases bone volume and uniformity of mineralization in aged ovariectomized rats. *Bone* 2005;37:87–95.
- [46] Boivin GY, Chavassieux PM, Santora AC, Yates J, Meunier PJ. Alendronate increases bone strength by increasing the mean degree of mineralization of bone tissue in osteoporotic women. *Bone* 2000;27(5): 687–94.

- [47] Boivin G, Vede S, Purdie DW, Compston JE, Meunier PJ. Influence of estrogen therapy at conventional and high doses on the degree of mineralization of iliac bone tissue: a quantitative microradiographic analysis in postmenopausal women. *Bone* 2005;36(3):562–7.
- [48] Boivin G, Lips P, Ott SM, Harper KD, Sarkar S, Pinette KV, et al. Contribution of Raloxifene and calcium and vitamin D3 supplementation to the increase of the degree of mineralization of bone in postmenopausal women. *J Clin Endocrinol Metab* 2003;88(9):4199–205.
- [49] Ruffoni D, Fratzl P, Roschger P, Klaushofer K, Weinkamer R. The bone mineralization density distribution as a fingerprint of the mineralization process. *Bone* 2007;40:1308–19.
- [50] Riggs BL, Hodgson SF, O'Fallon WM, Chao EYS, Wahner HW, Muhs JM, et al. Effect of fluoride treatment on fracture rate in postmenopausal women with osteoporosis. *N Engl J Med* 1990;322:802–9.
- [51] Fratzl P, Roschger P, Eschberger J, Abendroth B, Klaushofer K. Abnormal bone mineralization after fluoride treatment in osteoporosis: a small-angle X-ray scattering study. *J Bone Min Res* 1994;9:1541–9.
- [52] Kneissel M, Boyde A, Gasser JA. Bone tissue and its mineralization in aged estrogen-depleted rats after long-term intermittent treatment with parathyroid hormone (PTH) analog SDZ PTS 893 or human PTH(1–34). *Bone* 2001;28:237–50.
- [53] Rauch F, Glorieux FH. Osteogenesis imperfecta. *Lancet* 2004;363:1377–85.
- [54] Grabner B, Landis WJ, Roschger P, Rinnerthaler S, Peterlik H, Klaushofer K, et al. Age- and genotype-dependence of bone material properties in the osteogenesis imperfecta murine model (oim). *Bone* 2001;29:453–7.
- [55] Fratzl P, Paris O, Klaushofer K, Landis WJ. Bone mineralization in an osteogenesis imperfecta mouse model studied by small-angle X-ray scattering. *J Clin Invest* 1996;97:396–402.
- [56] Misof K, Landis WJ, Klaushofer K, Fratzl P. Collagen from the osteogenesis imperfecta mouse model (oim) shows reduced resistance against tensile stress. *J Clin Invest* 1997;100:40–5.
- [57] Misof BM, Roschger P, Baldini T, Raggio CL, Zraick V, Root L, et al. Differential effects of alendronate treatment on bone from growing osteogenesis imperfecta and wildtype mouse. *Bone* 2005;36:150–8.
- [58] Fratzl-Zelman N, Valenta A, Roschger P, Nader A, Gelb B, Fratzl P, et al. Decreased bone turnover and deterioration of bone structure in two cases of pycnodysostosis. *J Clin Endocrinol Metab* 2004;89:1538–47.
- [59] Misof BM, Roschger P, Tesch W, Baldock P, Valenta A, Meßmer P, et al. Targeted overexpression of vitamin D receptor in osteoblasts increases calcium concentration without affecting structural properties of bone mineral. *J Clin Endocrinol Metab* 2003;88:1150–6.
- [60] Tesch W, VandenBos T, Roschger W, Fratzl-Zelman N, Klaushofer K, Beertsen W, et al. Orientation of mineral crystallites and mineral density during skeletal development in mice deficient in tissue non-specific alkaline phosphatase. *J Bone Miner Res* 2003;18:117–25.
- [61] Roschger P, Matsuo K, Misof BM, Tesch W, Jochum W, Wagner EF, et al. Normal mineralization and nanostructure of sclerotic bone in mice overexpressing Fra-1. *Bone* 2004;34:776–82.
- [62] Fratzl P, Schreiber S, Klaushofer K. Bone mineralization as studied by small-angle X-ray scattering. *Conn Tissue Res* 1996;34:247–54.
- [63] Rinnerthaler S, Roschger P, Jakob HF, Nader A, Klaushofer K, Fratzl P. Scanning small angle X-ray scattering analysis of human bone sections. *Calcif Tissue Int* 1999;64(5):422–9.
- [64] Wagermaier W, Gupta HS, Gourrier A, Burghammer M, Roschger P, Fratzl P. Spiral twisting of fiber orientation inside bone lamellae. *BioInterphases* 2006;1:1–5.
- [65] Roschger P, Grabner BM, Rinnerthaler S, Tesch W, Kneissel M, Berzlanovich A, et al. Structural development of the mineralized tissue in the human L4 vertebral body. *J Struct Biol* 2001;136:126–36.
- [66] Fratzl P, Fratzl-Zelman N, Klaushofer K, Vogl G, Koller K. Nucleation and growth of mineral crystals in bone studied by small-angle X-ray scattering. *Calcif Tissue Int* 1991;48:407–13.
- [67] Zizak I, Roschger P, Paris O, Misof BM, Berzlanovich A, Bernstorff S, et al. Characteristics of mineral particles in the human bone/cartilage interface. *J Struct Biol* 2003;141:208–17.
- [68] Tesch W, Eidelman N, Roschger P, Goldenberg F, Klaushofer K, Fratzl P. Graded microstructure and mechanical properties of human dentin. *Calcif Tissue Int* 2001;69:147–57.
- [69] Gupta SH, Schratte S, Tesch W, Roschger P, Berzlanovich A, Schoeberl T, et al. Two different correlations between nanoindentation modulus and mineral content in the bone–cartilage interface. *J Struct Biol* 2005;149:138–48.
- [70] Gupta HS, Messmer P, Roschger P, Bernstorff S, Klaushofer K, Fratzl P. Synchrotron diffraction study of deformation mechanisms in mineralized tendon. *Phys Rev Lett* 2004;93(15):158101–1–4.
- [71] Gupta HS, Wagermaier W, Zickler GA, Aroush DRB, Funari SS, Roschger P, et al. Nanoscale deformation mechanisms in bone. *Nanoletters* 2005;5:2108–11.
- [72] Gupta HS, Seto J, Wagermaier W, Zaslansky P, Boesecke P, Fratzl P. Cooperative deformation of mineral and collagen in bone at the nanoscale. *PNAS* 2006;103(47):17741–17746.
- [73] Peterlik H, Roschger P, Klaushofer K, Fratzl P. From brittle to ductile fracture of bone. *Nat Mater* 2006;5:52–5.
- [74] Paschalis EP, Lyritis G, Skarantavos G, Shane E, Mendelsohn R, Boskey AL. Bone fragility and collagen cross-links. *J Bone Miner Res* 2004;19(12):2000–4.
- [75] Durchschlag E, Paschalis E, Zoehrer R, Roschger P, Fratzl P, Recker R, et al. Bone material properties in trabecular bone from human iliac crest biopsies after 3- and 5-year treatment with risedronate. *J Bone Miner Res* 2006;21:1581–90.
- [76] Kazanci M, Roschger P, Paschalis EP, Klaushofer K, Fratzl P. Bone osteonal tissues by Raman spectral mapping. *J Struct Biol* 2006;156(3):489–96.
- [77] Hofmann T, Heyroth F, Meinhard H, Fraenzel W, Raum K. Assessment of composition and anisotropic elastic properties of secondary osteon lamellae. *J Biomech* 2006;39:2282–94.